Journal of Sound and Vibration 329 (2010) 1274–1288

Contents lists available at ScienceDirect

Journal of Sound and Vibration

journal homepage: www.elsevier.com/locate/jsvi

On the design of structural junctions for the purpose of hybrid passive–active vibration control

Jonas L. Svensson *, Patrik B.U. Andersson, Wolfgang Kropp

Division of Applied Acoustics, Chalmers University of Technology, 41296 Göteborg, Sweden

ARTICLE INFO

Article history:
Received 22 June 2009
Received in revised form
27 October 2009
Accepted 2 November 2009
Handling Editor: A.V. Metrikine
Available online 28 November 2009

ABSTRACT

A theoretical investigation of wave scattering and the active modification of wave scattering at structural junctions is presented. A resonant and a non-resonant Euler–Bernoulli beam are coupled, and an external force is introduced at the junction. The external force is intended for feedforward control in order to manipulate the scattering properties at the junction. The purpose of the investigated control law is to make the junction non-reflective in the case of an incident bending wave. The control effort and the resulting power flow are investigated for different properties of the beams. By introducing damping in the resonant beam all incidence wave power is absorbed either passively, in the resonant beam, or actively, by the force. The results form the basis for a discussion of the possible benefits of using such a configuration for hybrid passive–active vibration control. The results show that for certain ratios of bending stiffness and mass the presented hybrid passive–active solution may offer advantages compared to purely passive or purely active solutions.

1. Introduction

Trusses and structural networks that contain junctions of slender beams appear as components in several types of constructions, such as satellites or vehicle bodies. An adequate knowledge of the vibration properties of such structures is essential in the design process. Slender beams can often be modelled as one-dimensional waveguides. Several papers have treated structural junctions of one-dimensional waveguides, e.g. [1,2]. An impedance mismatch at the junction will cause an incident wave-field to be partly transmitted and partly reflected. This can be described by two scattering matrices: one reflection and one transmission matrix. The dimensions of these matrices are determined by the number of wave types considered. A structural junction on a beam, undergoing pure bending motion, can be described by 2×2 matrices. The first row of the reflection matrix between two non-resonant beams was published by Cremer and Heckl [3], and the full matrices were derived by Mace [4]. Mei et al. derived the scattering matrices for a junction on a Timoshenko beam [5].

For several applications it is useful to control the vibrational behaviour at structural junctions, and thereby also control the wave propagation into the connected beams. In a series of studies, Miller et al. presented different control laws for junction control. The studied control laws included manipulating the junction's scattering properties and optimal controllers for power absorption [6–8]. Scheuren presented two experimental studies investigating active reflection and transmission control. Two sensors, in the far-field, were used to estimate the amplitudes of a positively and a negatively propagating bending wave. In the first study, an actuator was placed at a free end and driven to suppress the wave propagating away from the end, hence creating a non-reflective termination [9]. In the second study the wave amplitude was used as the reference signal to drive an actuator to block the incident wave, thus cancelling the transmission past the control point [10]. Non-reflecting beam terminations have also been studied e.g. in [11,12] for Euler–Bernoulli beams, and in [13] for Timoshenko beams. The use of active control in order to cancel bending waves has been studied e.g. in [14–17].

* Corresponding author. Tel.: +46 31 772 2209; fax: +46 31 772 2212.
E-mail address: jonas.svensson@chalmers.se (J.L. Svensson).

0022-460X/$ - see front matter © 2009 Elsevier Ltd. All rights reserved.
doi:10.1016/j.jsv.2009.11.002

Nomenclature

EI	bending stiffness
F	shear force
M	bending moment
$\mathbf{C}$	matrix containing geometric relations
$\mathbf{Z}$	impedance matrix
$\mathbf{Q}$	force vector
W	power
a	wave amplitude
$\mathbf{a}$	wave amplitude vector
v	normal velocity
w	rotational velocity
$\mathbf{u}$	velocity vector
r	reflection coefficient
$\mathbf{r}$	reflection matrix
z	impedance element
k	wavenumber
kl	wavenumber length product
m'	mass per unit length
x	coordinate
e	exponential
j	imaginary unit

Greek letters

β^2	bending stiffness ratio
γ^2	mass ratio
χ	the product of β, δ and χ
δ	complex stiffness parameter
η	loss factor
ξ	normal displacement
ω	angular frequency
$\mathbf{\Psi}$	propagation matrix
Ω	reflection factor denominator

Subscripts

p	propagating wave
N	near field
0	evaluated at $x=0$

Superscripts

$+$	positively travelling
$-$	negatively travelling
$*$	complex conjugate
diss	dissipated
H	Hermitian transpose
dp	driving-point
act	active
pass	passive

Svensson et al. theoretically studied the influence of beam properties on the control effort and power flow, for different control laws concerning junction control [18]. The beams in this study were non-dissipative and semi-infinite; the latter implies that no resonance phenomena could be studied. The same authors made a theoretical study of active control at a structural junction with an impedance formulation [19]. An active force was used to match the impedance at the junction of an Euler–Bernoulli beam and a sandwich composite. The intention was to investigate the possibility of using such a solution for hybrid passive–active vibration control. Configurations based on these principles have been used for airborne sound absorption [20–23]. The results from [19] showed that at frequencies where the sandwich composite has internal resonances, the control effort might be high and the active force may inject a substantial amount of power into the composite. For a possible application of hybrid passive–active vibration control this is obviously unfortunate. Several publications have treated hybrid passive–active vibration control in different variations. Active constrained layers (ACL) [24,25] and variations of ACL [26–28], have been studied extensively during recent years. There has also been research on splitting ACL into a passive constrained layer and pure active control [29,30]. A discussion of different passive–active vibration control configurations can be found in [31]. Despite a substantial amount of research, there seems to be no final answer as to which is the most effective way to combine active and passive vibration control.

The purpose of the presented paper is to answer some of the questions raised in [19]. Based on the impedance formulation developed in that study, the junction between a non-resonant and a highly dissipative, resonant Euler–Bernoulli beam is investigated. An active force is employed to make the junction non-reflective, and thus all incident wave power is absorbed, either actively or passively. The influence of the beam properties on the power flow across the junction and on the control effort is investigated. The objective is to investigate whether the properties of the resonant beam can be chosen in a way which is beneficial for hybrid passive–active vibration control and thus avoiding the high control effort and power injection which may occur at some resonances, as discovered in [19].

2. Theoretical model

2.1. Euler–Bernoulli beam

Euler–Bernoulli theory describes the vibration field on one-dimensional structural waveguides undergoing pure bending motion. The homogenous version of the governing differential equation is given by

$$\mathrm{EI}\frac{\partial^4}{\partial x^4}\xi(x,t)+m'\frac{\partial^2}{\partial t^2}\xi(x,t)=0, \tag{1}$$

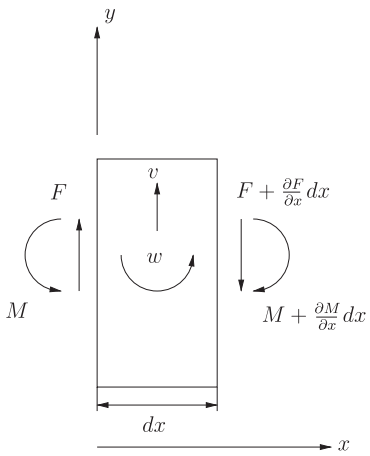

Fig. 1. A beam-element of length d*x*. v indicates the translational velocity, w the rotational velocity, M the bending moment and F the shear force.

where ξ is the displacement, m' the mass per unit length and EI the bending stiffness, x and t the length and time coordinate, respectively. Eq. (1) assumes that m' and EI are uniform along the x-axis. The complex translational velocity field on an Euler–Bernoulli beam undergoing harmonic motion can be described as the sum of four wave components according to

$$v(x) = a_p^+ \mathrm{e}^{-\mathrm{j}kx} + a_N^+ \mathrm{e}^{-kx} + a_p^- \mathrm{e}^{\mathrm{j}kx} + a_N^- \mathrm{e}^{kx}, \tag{2}$$

where a_p^+ and a_p^- are the velocity amplitudes of bending waves propagating in positive and negative direction, respectively, a_N^+ and a_N^- are the velocity amplitudes bending near-fields decaying in positive and negative direction, respectively; j represents the imaginary unit, k represents bending wavenumber and is defined as

$$k = \sqrt{\omega}\sqrt[4]{\frac{m'}{\mathrm{EI}}}. \tag{3}$$

The time dependence $\mathrm{e}^{\mathrm{j}\omega t}$ in Eq. (2) has been suppressed for brevity. The velocity, v, is related to the displacement, ξ, through a differentiation in time. As this paper is treating bending waves and bending near-fields exclusively, they will be referred to from now on simply as waves and near-fields.

The translational velocity can be related to rotational velocity (w), bending moment (M), and shear force (F) using the following relations:

$$w = \frac{\partial v}{\partial x}, \qquad M = \frac{-\mathrm{EI}}{\mathrm{j}\omega}\frac{\partial w}{\partial x}, \qquad F = -\frac{\partial M}{\partial x}, \tag{4a,b,c}$$

where the sign convention is chosen according to Fig. 1. The translational and rotational velocities may be expressed as the sum of the wave components travelling in positive and negative direction, respectively

$$\mathbf{u}(x) = \mathbf{u}^+(x) + \mathbf{u}^-(x), \tag{5}$$

where

$$\mathbf{u}(x) = \begin{Bmatrix} v(x) \\ w(x) \end{Bmatrix}, \tag{6}$$

and

$$\mathbf{u}(x)^+ = \mathbf{C}^+ \boldsymbol{\Psi}^+(x)\mathbf{a}^+, \tag{7a}$$

$$\mathbf{u}(x)^- = \mathbf{C}^- \boldsymbol{\Psi}^-(x)\mathbf{a}^-, \tag{7b}$$

where

$$\mathbf{C}^+ = \begin{bmatrix} 1 & 1 \\ -\mathrm{j}k & -k \end{bmatrix}, \quad \mathbf{C}^- = \begin{bmatrix} 1 & 1 \\ \mathrm{j}k & k \end{bmatrix}, \tag{8a,b}$$

$$\boldsymbol{\Psi}^+(x) = \begin{bmatrix} \mathrm{e}^{-\mathrm{j}kx} & 0 \\ 0 & \mathrm{e}^{-kx} \end{bmatrix}, \quad \boldsymbol{\Psi}^-(x) = \begin{bmatrix} \mathrm{e}^{\mathrm{j}kx} & 0 \\ 0 & \mathrm{e}^{kx} \end{bmatrix}, \tag{9a,b}$$

and

$$\mathbf{a}^+ = \begin{Bmatrix} a_p^+ \\ a_N^+ \end{Bmatrix}, \quad \mathbf{a}^- = \begin{Bmatrix} a_p^- \\ a_N^- \end{Bmatrix}. \tag{10a,b}$$

The translational and rotational velocities can be related to the internal bending moment and shear force through the characteristic impedance matrices according to

$$\begin{Bmatrix} F(x) \\ M(x) \end{Bmatrix} = \tilde{\mathbf{Z}}^+ \mathbf{u}^+(x) + \tilde{\mathbf{Z}}^- \mathbf{u}^-(x), \tag{11}$$

where

$$\tilde{\mathbf{Z}}^+ = \frac{\mathrm{EI}}{\omega} \begin{bmatrix} (1+\mathrm{j})k^3 & k^2 \\ k^2 & (1-\mathrm{j})k \end{bmatrix}, \tag{12a}$$

$$\tilde{\mathbf{Z}}^- = \frac{\mathrm{EI}}{\omega} \begin{bmatrix} -(1+\mathrm{j})k^3 & k^2 \\ k^2 & (\mathrm{j}-1)k \end{bmatrix}. \tag{12b}$$

These characteristic impedance matrices were first derived in [32], and represent the impedance associated with a freely propagating wave and near-field.

2.2. Structural junctions

If wave components travelling in positive direction enter a boundary or discontinuity they will reflect wave components travelling in the opposite direction. The relation between the wave components in positive and negative direction is determined by the reflection matrix according to

$$\mathbf{a}^- = \mathbf{r}\mathbf{a}^+. \tag{13}$$

The reflection matrix is determined by the specific boundary conditions at the considered discontinuity or termination.

Consider a semi-infinite beam, with the boundary located at the origin of a Cartesian coordinate system; see Fig. 2. A semi-infinite beam is non-resonant, which in this case means that the wave components travelling in negative direction are not reflected. The boundary conditions can be specified through an impedance matrix which relates the translational and rotational velocities to the shear force and bending moment at the boundary according to

$$\mathbf{Q}_0 = \hat{\mathbf{Z}}\mathbf{u}_0, \tag{14}$$

where

$$\mathbf{Q}_0 = \begin{Bmatrix} F(x=0) \\ M(x=0) \end{Bmatrix}, \quad \mathbf{u}_0 = \begin{Bmatrix} v(x=0) \\ w(x=0) \end{Bmatrix}. \tag{15a,b}$$

The matrix, $\hat{\mathbf{Z}}$, is referred to as the junction impedance matrix, and represents an arbitrary junction. The reflection matrix for the junction can be expressed in terms of the characteristic impedance matrices and the junction impedance matrix, according to

$$\mathbf{r} = (\mathbf{C}^-)^{-1}(\tilde{\mathbf{Z}}^- - \hat{\mathbf{Z}})^{-1}(\hat{\mathbf{Z}} - \tilde{\mathbf{Z}}^+)\mathbf{C}^+. \tag{16}$$

The matrices $\tilde{\mathbf{Z}}^+$ and $\tilde{\mathbf{Z}}^-$ are defined in Eqs. (12a) and (12b); and $\mathbf{C}^+$ and $\mathbf{C}^+$ are defined in Eqs. (8a) and (8b). Eq. (16) was derived in [19]. If e.g. the non-resonant beam is terminated by a free end, the reflection matrix can be found by inserting the null matrix as the junction impedance matrix in Eq. (16). Examples of different junction impedance matrices and the corresponding reflection matrices are given in [33]. Though the four elements in the junction impedance matrix characterise a junction uniquely, the matrix can be approximated by the elements in the main diagonal [34].

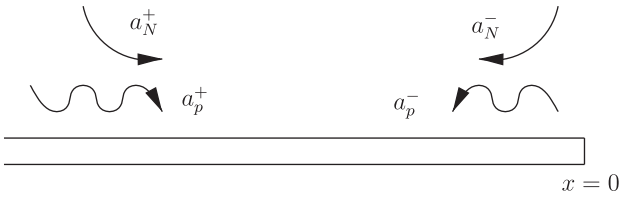

Fig. 2. Schematic drawing of a non-resonant beam.

If the junction impedance matrix represents a system that contains losses, e.g. a dashpot, any incident wave-field will be partly dissipated at the junction. The dissipated power can be calculated according to

$$W^{\mathrm{diss}} = \tfrac{1}{2}\mathrm{Re}\{\mathbf{u}_0^{\mathrm{H}}\hat{\mathbf{Z}}\mathbf{u}_0\}, \tag{17}$$

where the superscript, H, denotes Hermitian transpose.

2.3. The driving-point impedance matrix of a free–free Euler–Bernoulli beam

The driving-point impedance matrix represents the impedances encountered by an external force and moment excitation, respectively. The matrix depends on the properties of the beam and its boundary conditions. The driving-point impedance matrix at the left boundary of an Euler–Bernoulli beam with a free–free boundary condition is given by

$$\mathbf{Z}^{\mathrm{dp}} = \frac{\mathrm{jEI}}{\omega}\frac{\quad}{\cos kl\cosh kl+1}\begin{bmatrix} k^3(\tan kl+\tanh kl) & k^2\tanh kl\tan kl \\ k^2\tanh kl\tan kl & k(\tan kl-\tanh kl)\end{bmatrix}, \tag{18}$$

where kl is the product of the wavenumber and length, in airborne sound referred to as the Helmholtz number. A beam can be modelled to have internal losses using a complex modulus according to $E=E'(1+\mathrm{j}\eta)$, where E' is Young's modulus and η is the loss factor. This will in turn result in a complex wavenumber according to

$$k \approx k'\left(1-\mathrm{j}\frac{\eta}{4}\right), \tag{19}$$

where k' is the wavenumber defined in Eq. (3). Inserting this complex wavenumber into the tangential functions in the driving-point impedance matrix in Eq. (18) yields

$$\tan(kl) = \frac{\tan(k'l)-\mathrm{j}\tanh\left(k'l\frac{\eta}{4}\right)}{1+\mathrm{j}\tan(k'l)\tanh\left(k'l\frac{\eta}{4}\right)}, \tag{20a}$$

$$\tanh(kl) = \frac{\tanh(k'l)-\mathrm{j}\tan\left(k'l\frac{\eta}{4}\right)}{1-\mathrm{j}\tanh(k'l)\tan\left(k'l\frac{\eta}{4}\right)}. \tag{20b}$$

Consider the case where there is at least some damping (i.e. $\eta>0$) and where the beam is long in comparison to the wavelength (i.e. $k'l\gg 1$). Based on these assumptions, the term $\tanh(k'l)$ will be close to unity and thus Eqs. (20a) and (20b) will reduce to $-\mathrm{j}$ and 1, respectively. Under the same assumptions $\cos kl\cosh kl\gg 1$. Thus, as $k'l$ increases the matrix in Eq. (18) will approach the characteristic impedance matrix for wave components travelling in positive direction; see Eq. (12a).

2.4. Reflection efficiency of the junction

The resonant Euler–Bernoulli beam, described by the driving-point impedance matrix in Eq. (18), can be coupled to the non-resonant beam in Fig. 2, resulting in the configuration given in Fig. 3 without the active force at the junction. The reflection matrix for this junction can be obtained by inserting the driving-point impedance matrix in Eq. (18), into Eq. (16). The resulting reflection matrix is given by

$$\mathbf{r} = \frac{1}{\Omega}\begin{bmatrix} r_{11} & r_{12} \\ r_{21} & r_{22}\end{bmatrix}, \tag{21}$$

where

$$r_{11} = -\mathrm{j}\chi^2\det(\check{\mathbf{Z}}) - \sqrt{2\chi}(\gamma\check{z}_{11}-\beta\delta\check{z}_{22})+\chi(\check{z}_{12}+\check{z}_{21})-\mathrm{j}, \tag{22a}$$

$$r_{12} = (1+\mathrm{j})(1-\chi^2\det(\check{\mathbf{Z}})), \tag{22b}$$

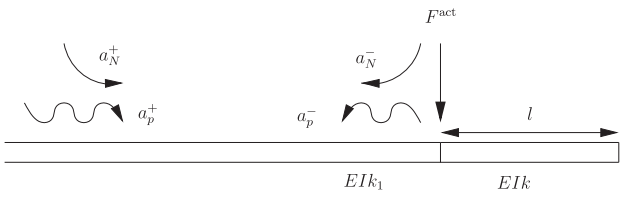

Fig. 3. Schematic drawing of the junction of the non-resonant and the resonant beams, showing the waves present on the non-resonant beam and an active force at the junction.

$$r_{21} = (1 - \mathrm{j})(1 - \chi^2 \det(\check{\mathbf{Z}})), \tag{22c}$$

$$r_{22} = \mathrm{j}\chi^2 \det(\check{\mathbf{Z}}) - \sqrt{2\chi}(\gamma \check{z}_{11} - \beta\delta \check{z}_{22}) - \mathrm{j}\chi(\check{z}_{12} + \check{z}_{21}) + \mathrm{j}, \tag{22d}$$

$$\Omega = \chi^2 \det(\check{\mathbf{Z}}) + \sqrt{2\chi}(\gamma \check{z}_{11} + \beta\delta \check{z}_{22}) + \chi(\check{z}_{12} + \check{z}_{21}) + 1, \tag{23}$$

where $\det(\check{\mathbf{Z}})$ denotes the determinant of $\check{\mathbf{Z}}$. The matrix $\check{\mathbf{Z}}$ is defined as

$$\check{\mathbf{Z}} = \frac{\cos kl \cosh kl}{\cos kl \cosh kl + 1} \begin{bmatrix} \frac{\sqrt{2}}{1+\mathrm{j}}(\tan kl + \tanh kl) & \tanh kl \tan kl \\ \tanh kl \tan kl & \frac{\sqrt{2}}{1-\mathrm{j}}(\tan kl - \tanh kl) \end{bmatrix} \tag{24}$$

and

$$\beta^2 = \frac{\mathrm{EI}_2}{\mathrm{EI}_1}, \quad \gamma^2 = \frac{m_2'}{m_1'}, \quad \delta^2 = (1 + \mathrm{j}\eta), \quad \chi = \beta\delta\gamma, \tag{25a,b}$$

Here the subscripts 1 and 2 on EI and m' refer to the non-resonant and resonant beam, respectively. The loss factor η is given no subscript as only the resonant beam in this case contains losses. The impedance matrix $\check{\mathbf{Z}}$ (Eq. (24)) is dimensionless and similar to the matrix $\mathbf{Z}^{\mathrm{dp}}$ (Eq. (18)).

For vibration control purposes it might be interesting to maximise the absorption of vibrational power at the junction, i.e. minimise Eq. (17). If only an incident bending wave (and no near-field) is considered, minimising Eq. (17) will be equivalent to minimising the reflection efficiency of the (1,1) element of the reflection matrix, i.e. minimising $10\log_{10}(|r_{11}|^2)$. The amount of incoming wave power that is absorbed at the junction will depend on the properties of the beams.

2.4.1. Behaviour of the impedance matrices

Figs. 4 and 5 show the magnitude and the phase of the impedance elements in the junction impedance matrix and the characteristic impedance matrix as functions of $k'l$. The beam properties were chosen as $\mathrm{EI}_1 = \mathrm{EI}_2 = 5 \times 10^{10}\,\mathrm{N\,m^2}$, $m_1' = m_2' = 12\,\mathrm{kg/m}$ and $\eta = 0.3$, hence $\beta = \gamma = 1$ and $\delta^2 = 1 + 0.3\mathrm{j}$. The reason for the choice of properties is just to have a few resonances in the investigated range of kl. Figs. 4 and 5 show that for high values of $k'l$, the magnitude of the junction impedance matrix approaches the characteristic impedance matrix which causes the reflection efficiency to decrease. The phase, however, deviates slightly even for high values of $k'l$, due to the difference in loss factor. Thus the reflection

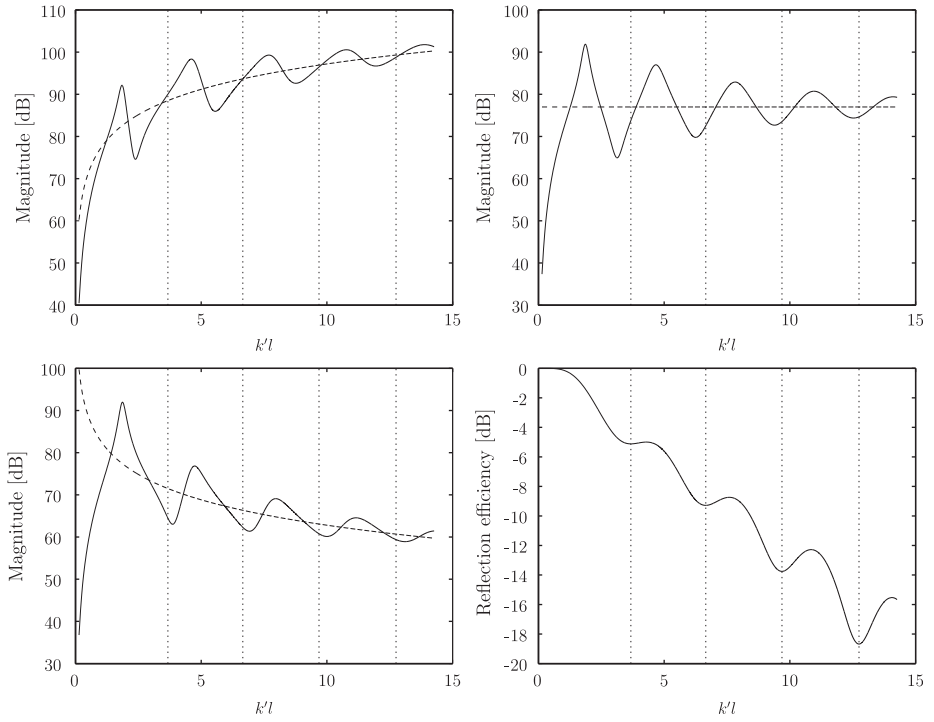

Fig. 4. The magnitude of the impedance elements and the reflection factor (r_{11}); —: Junction impedance ($\hat{\mathbf{Z}}$); - - -: Characteristic impedance ($\tilde{\mathbf{Z}}^+$). Top left: $\hat{z}_{11}$; top right: $\hat{z}_{12}$, $\hat{z}_{21}$; bottom left: $\hat{z}_{22}$; bottom right: r_{11}. The vertical dotted lines indicate where local minima occur in the reflection efficiency. $\mathrm{EI}_1 = \mathrm{EI}_2 = 5 \times 10^{10}\,\mathrm{N\,m^2}$, $m_1' = m_2' = 12\,\mathrm{kg/m}$.

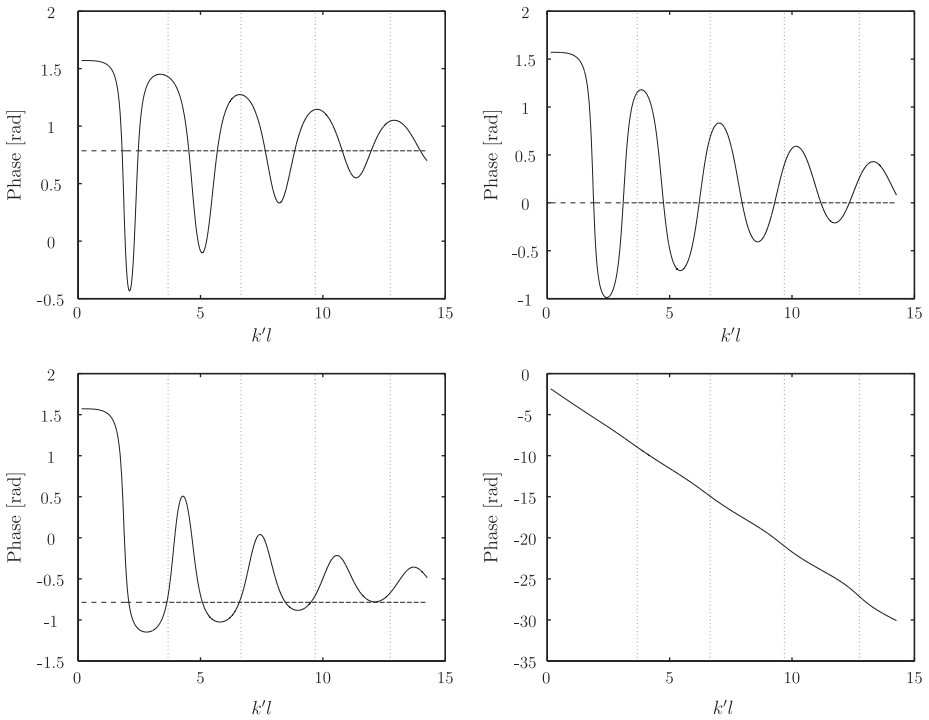

Fig. 5. The phase of the impedance elements and the reflection factor r_{11}; —: Junction impedance ($\hat{\mathbf{Z}}$); - - -: Characteristic impedance ($\tilde{\mathbf{Z}}^+$). Top left: $\hat{z}_{11}$; top right: $\hat{z}_{12}$, $\hat{z}_{21}$; bottom left: $\hat{z}_{22}$; bottom right: r_{11}. The vertical dotted lines indicate where local minima occur in the reflection efficiency. $\mathrm{EI}_1 = \mathrm{EI}_2 = 5 \times 10^{10}\,\mathrm{N\,m^2}$, $m_1' = m_2' = 12\,\mathrm{kg/m}$.

efficiency does not approach negative infinity but a finite value (approximately −28 dB). Following the discussion above, a lower loss factor in the resonant beam would actually give a lower reflection efficiency for high values of $k'l$. The value that the reflection efficiency asymptotically approaches for high values of $k'l$ can be found by replacing the driving-point impedance matrix (Eq. (18)), in Eq. (16) by the equivalent characteristic impedance matrix for wave components travelling in positive direction (Eq. (12a)). Figs. 4 and 5 show another interesting aspect. At positions where the reflection efficiency reaches local minima, the magnitudes of $\check{z}_{11}$,$\check{z}_{12}$ and $\check{z}_{21}$ are close to the corresponding elements in the characteristic impedance matrix. However, the magnitude of $\check{z}_{22}$ diverges substantially from $\tilde{z}^+_{22}$. The opposite is true for the phase. This highlights an important aspect, namely that, in contrast to the case of longitudinal waves, there is no simple relationship between the impedances which will give a low reflection efficiency of r_{11}. It is the entire expression in Eq. (21) that needs to be considered. Thus, impedance matching becomes much more difficult compared to the case of longitudinal waves.

2.4.2. *Influence of damping*

Consider the case when the beams have identical bending stiffness and mass, i.e. $\beta = \gamma = 1$. Note that identical mass and stiffness do not necessarily mean identical material or geometry. A difference in density between the two beams can be compensated for by the cross-sectional height, and a difference in Young's modulus can be compensated for by the cross-sectional width. For the case $\beta = \gamma = 1$, the loss factor is the only property that differs between the beams. The reflection efficiency as a function of loss factor for different values of $k'l$ is plotted in Fig. 6. The figure shows that as $k'l = 1$ and 5 the reflection efficiency decreases, i.e. the absorption increases, with an increasing loss factor in the range $\eta = 0{-}0.5$. However, as $k'l = 50$ and 100 there is an optimal choice of loss factor in order to maximise the absorption of incident wave power. A loss factor which is lower than this optimal value means that the wave power that enters the resonant beam is less dissipated while a higher loss factor causes a greater impedance mismatch at the junction and thus a higher reflection efficiency. This highlights the fact that the highest loss factor does not always result in optimal absorption. A loss factor with a particular frequency characteristic could in this case maximise the absorption of incident wave power for a broader frequency range, i.e. a broader range of kl.

2.4.3. *Influence of stiffness, mass and length*

In order to investigate the influence of the stiffness, mass and length of the resonant beam, the reflection efficiency is plotted as a function of the mass ratio (γ^2) and kl for different values of stiffness ratio (β^2) in Figs. 7–9. The loss factor is chosen as 0.3, thus $\delta^2 = 1 + 0.3\mathrm{j}$. The reason for this choice is the desire to investigate a highly damped (but not necessarily optimally damped) resonant beam, as it is intended for vibration control. Note that it is the real part of kl (i.e. $k'l$) which is

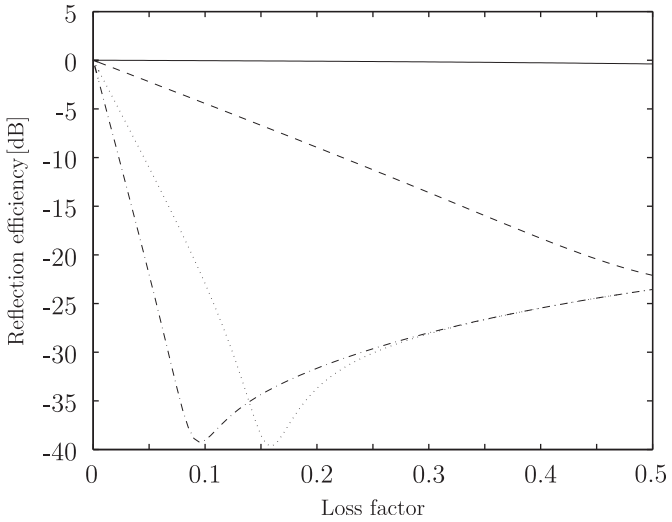

Fig. 6. The reflection efficiency as a function of the loss factor, for the case $\beta^2=\gamma^2=1$. —: $k'l=1$; - - -: $k'l=10$; ····· : $k'l=50$; - · - : $k'l=100$.

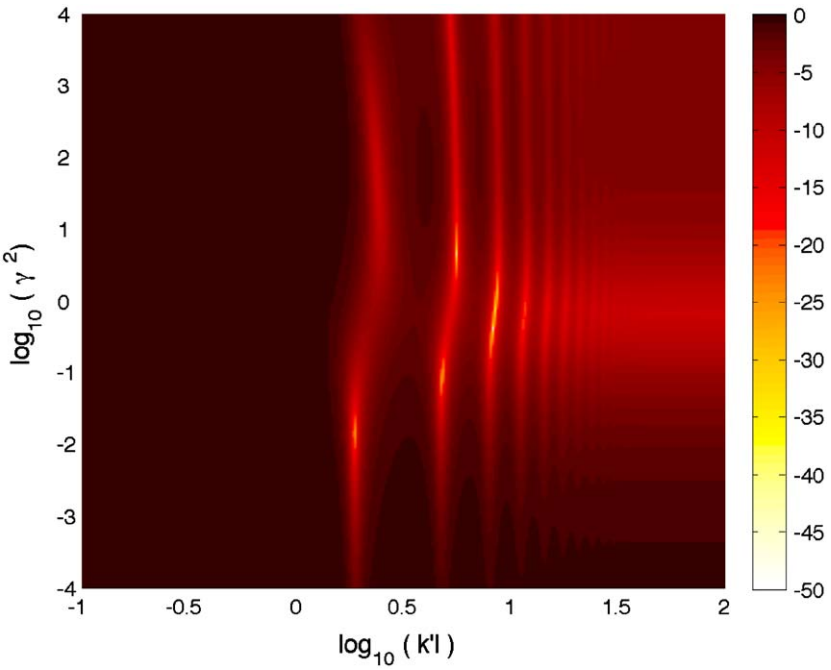

Fig. 7. The reflection efficiency in dB as a function of γ and kl, for $\beta^2=0.1$.

indicated on the x-axis in the figures. The relation between the real and the imaginary part of kl is fixed through the choice of the loss factor according to Eq. (19).

Fig. 8 shows that if $\beta=\gamma=1$, the reflection efficiency is low for large values of kl. This can be expected because, when there is no significant difference in mass and stiffness between the beams, and the resonant beam is long compared to the wavelength, most incident wave power will enter and be dissipated in the resonant beam. The same phenomenon can be seen in Eqs. (20a) and (20b), i.e. for $\beta=\gamma=1$ and $k'l\gg1$ the driving-point impedance matrix for the resonant beam approaches the characteristic impedance matrix for wave components travelling in positive direction. Note that the resonant beam contains damping and the non-resonant does not. Hence even though $\beta=\gamma=1$, the beams still have different properties given by δ.

If $\beta\neq1$, the reflection efficiency approaches a local minimum for $\gamma\neq1$ and $k'\gg1$. The value of the minima is determined by the ratio of bending stiffnesses and masses, e.g. in Fig. 7 ($\beta^2=0.1$) the reflection efficiency asymptotically approaches approximately -11 dB for $k'l\gg1$ and $\gamma^2\approx0.9$. For all Figs. 7–9, the reflection efficiency reach minima for certain specific

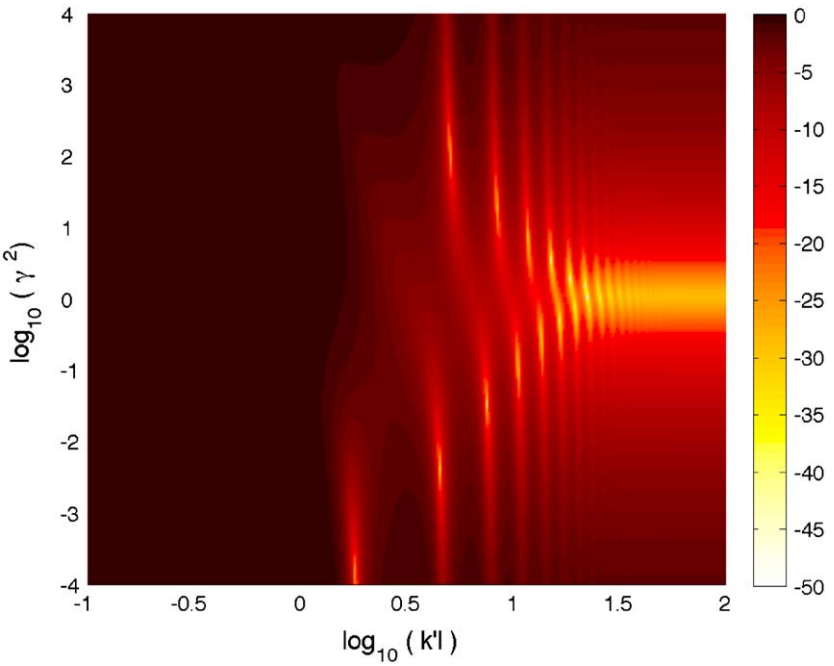

Fig. 8. The reflection efficiency in dB as a function of γ and kl, for $\beta^2 = 1$.

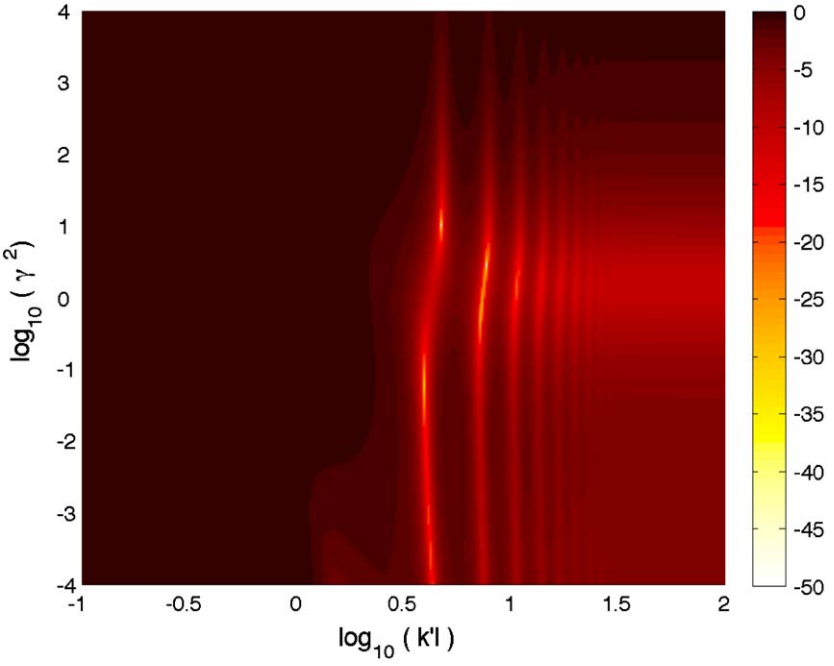

Fig. 9. The reflection efficiency in dB of a function of γ and kl, for $\beta^2 = 10$.

values of γ and kl. This indicates that for each mass and stiffness ratio there is a frequency where the absorption of incident wave power is maximum. This effect can be compared to the principle employed by tuned vibration absorbers; see e.g. [35].

Figs. 7–9 also show that for small values of kl the reflection efficiency is close to 0 dB (i.e. all incident power is reflected), independently of β and γ. This seems reasonable since when kl approaches zero, the junction approaches one of the four ideal termination cases, all which have a reflection efficiency of 0 dB. If kl is a non-zero number, the

four ideal termination cases can be obtained by allowing β and γ approach their limits. If $\beta\to 0$ and $\gamma\to 0$, the junction approaches a free end; if $\beta\to\infty$ and $\gamma\to\infty$, the junction approaches a clamped end; if $\beta\to\infty$ and $\gamma\to 0$, the junction approaches a guided termination; and finally if $\beta\to 0$ and $\gamma\to\infty$, the junction approaches a simply supported termination.

3. Introducing active control at the beam junction

The reflection efficiency is close to 0 dB for large regions in Figs. 7–9, which is unfortunate for vibration control purposes. Active control may be used in order to achieve a higher absorption of incident wave power in these cases. External forces and moments, for vibration control purposes, may be introduced in the formulation. This is achieved by dividing the junction impedance matrix, $\hat{\mathbf{Z}}$, into a passive and an active part according to

$$\hat{\mathbf{Z}} = \mathbf{Z}^{\mathrm{act}} + \mathbf{Z}^{\mathrm{pass}}, \tag{26}$$

where

$$\mathbf{Z}^{\mathrm{act}} = \begin{bmatrix} z_{11}^{\mathrm{act}} & z_{12}^{\mathrm{act}} \\ z_{21}^{\mathrm{act}} & z_{22}^{\mathrm{act}} \end{bmatrix}. \tag{27}$$

The active impedance matrix relates two possible modes of sensing (translational and rotational velocity at the junction) to two possible modes of actuation (force and moment at the junction) according to

$$\mathbf{Q}^{\mathrm{act}} = \mathbf{Z}^{\mathrm{act}}\mathbf{u}_0, \tag{28}$$

where

$$\mathbf{Q}^{\mathrm{act}} = \begin{Bmatrix} F^{\mathrm{act}} \\ M^{\mathrm{act}} \end{Bmatrix}. \tag{29}$$

The active force and moment will alter the total junction impedance matrix for a specific control purpose. In this way the active force and moment will manipulate the reflection matrix at the junction. In order to control all four elements in the reflection matrix, all four elements in the active impedance matrix have to be chosen appropriately. If the control law is to only control one element of the reflection matrix, it is necessary to employ only one element of the active impedance matrix, while the rest may be zero. A specific control law can be derived by first inserting Eq. (26) into (16), and then specify the desired constraints on the reflection matrix and solve for $\mathbf{Z}^{\mathrm{act}}$.

3.1. A non-reflective junction

A control law that may be of interest is the one that creates a non-reflective junction. Non-reflective junctions have been studied e.g. in [9,12,18] for an incident wave and in [11,19] for incident wave and near-field. To avoid any reflection of a bending wave in the latter case (i.e. $r_{11}=r_{12}=0$), two elements in the active impedance matrix have to be given appropriate values. To avoid a reflected wave in the former case (i.e. $r_{11}=0$), only one element in the active impedance matrix is needed. Any of the four elements may be used. An obvious choice would be to use the (1,1) element of the active impedance matrix, because sensors that measure translational velocity and actuators that apply forces have been successfully implemented in experimental investigations of active control, e.g. [36]. Actually most commonly (as in the cited publication) the acceleration is measured, the acceleration can then be integrated in order to acquire an estimate of the velocity. See Ref. [37] for an extensive discussion of different actuators for active vibration control. In order to obtain $r_{11}=0$, z_{11}^{act} is required to be

$$z_{11}^{\mathrm{act}} = -\frac{k_1^3 \mathrm{EI}_1(1+\mathrm{j})}{\omega}\cdot\frac{\chi^2\det(\check{\mathbf{Z}}) - \mathrm{j}\sqrt{2\chi}(\gamma\check{z}_{11} - \beta\delta\check{z}_{22}) - \chi(\check{z}_{21}+\check{z}_{12})+1}{\sqrt{2\chi}\beta\delta\check{z}_{22} - 2\mathrm{j}}. \tag{30}$$

In this case all incident wave power is dissipated, either by the active force or in the resonant beam. The active force is found by multiplying z_{11}^{act} by the translational velocity at the junction according to

$$F^{\mathrm{act}} = z_{11}^{\mathrm{act}} v(x=0), \tag{31}$$

where

$$v(x=0) = a_p^+(1 + r_{11}^{\mathrm{act}} + r_{21}^{\mathrm{act}}). \tag{32}$$

The superscript (act) on the elements in the reflection matrix indicate that they are manipulated by the active force. Through the specified control law $r_{11}^{\mathrm{act}}=0$. Inserting the active impedance matrix, corresponding to the control law in Eq. (30), into Eq. (16) yields

$$r_{21}^{\mathrm{act}} = \frac{2\mathrm{j} + 2\chi\check{z}_{21} - \sqrt{2\chi}\beta\delta\check{z}_{22}(1+\mathrm{j})}{2\mathrm{j} - 2\chi\check{z}_{21} - \sqrt{2\chi}\beta\delta\check{z}_{22}(1-\mathrm{j})}. \tag{33}$$

Thus, for an incident wave the total translational velocity at the non-reflective junction can be found. Substituting Eq. (33) into Eq. (31) yields

$$F^{\mathrm{act}} = \frac{a_p^+ k_1^3 \mathrm{EI}_1(1-\mathrm{j})}{\omega} \cdot \frac{\chi^2 \det(\check{\mathbf{Z}}) - \mathrm{j}\sqrt{2\chi}(\gamma \check{z}_{11} - \beta\delta\check{z}_{22}) - \chi(\check{z}_{21}+\check{z}_{12})+1}{\mathrm{j}\chi\check{z}_{21} + \sqrt{2\chi}\beta\delta\check{z}_{22}\frac{1}{2}(1+\mathrm{j})+1}. \tag{34}$$

This is the force which is required in order to achieve a non-reflection junction in this case. It is proportional to the amplitude of the incoming wave and the proportionality constant is determined by the properties of the two beams and the frequency. This control law assumes that the sensor and actuator are ideal.

3.2. Control effort

The matrix $\check{\mathbf{Z}}$, Eq. (24), is dimensionless and solely dependent on the parameter kl. If the force in Eq. (34) is normalised by the term $a_p^+ k_1^3 \mathrm{EI}_1(1-\mathrm{j})/\omega$, the control law depends on the parameters: β, γ, δ and kl. The normalisation term is the force required in order to achieve a non-reflective junction at a free end. This force can be found by letting the impedance elements in Eq. (34) approaches zero. The normalisation provides a good reference for evaluating the control effort, as 0 dB implies that the control effort is equal to that of cancelling the reflection at a free end. The normalised force level are plotted as a functions of γ and kl for different values of β and a loss factor of 0.3 (i.e. $\delta^2 = 1+0.3\mathrm{j}$) in Figs. 10–12.

Figs. 10–12 show that for a given γ, the control effort generally increases as β increases. More force is required to induce the required velocity if the resonant beam has a larger mass.

Figs. 10–12 show that the control effort is similar to that of cancelling the reflection at a free end, i.e. 0 dB, as γ decreases. The reason is that, for the investigated values of β (relatively low values), the junction approaches a termination similar to a free end as γ decreases. The figures show that some parameter combinations that give a control effort that is lower than the control effort for cancelling the reflection at a free end (< 0 dB). An example of this can be found in Fig. 11 for $\gamma = 1$ and a large value of kl. For these parameter combinations there is a low passive reflection efficiency; see Fig. 8. If the passive junction dissipates most of the incident wave, only a small force is required to cancel the remaining reflection. This indicates that choosing the properties of the resonant beam corresponding to these parameters is beneficial for a hybrid passive–active vibration control configuration. This means that the control effort is lower than that of absorbing the incident wave power at a free end, and the active control absorbs the remaining power, which is not dissipated by the purely passive junction.

3.3. Active power flow

The active power, i.e. the power injected or absorbed by the active force, can be calculated according to

$$W^{\mathrm{act}} = \tfrac{1}{2}\mathrm{Re}\{F^{\mathrm{act}} v^*(x=0)\}, \tag{35}$$

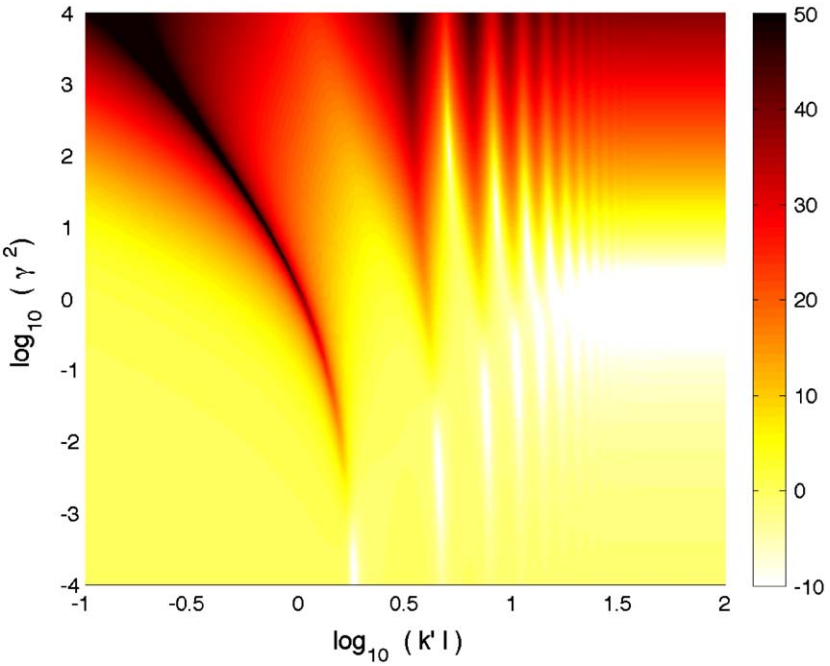

Fig. 10. The normalised active force in dB as a function of γ and kl, for $\beta^2 = 0.1$.

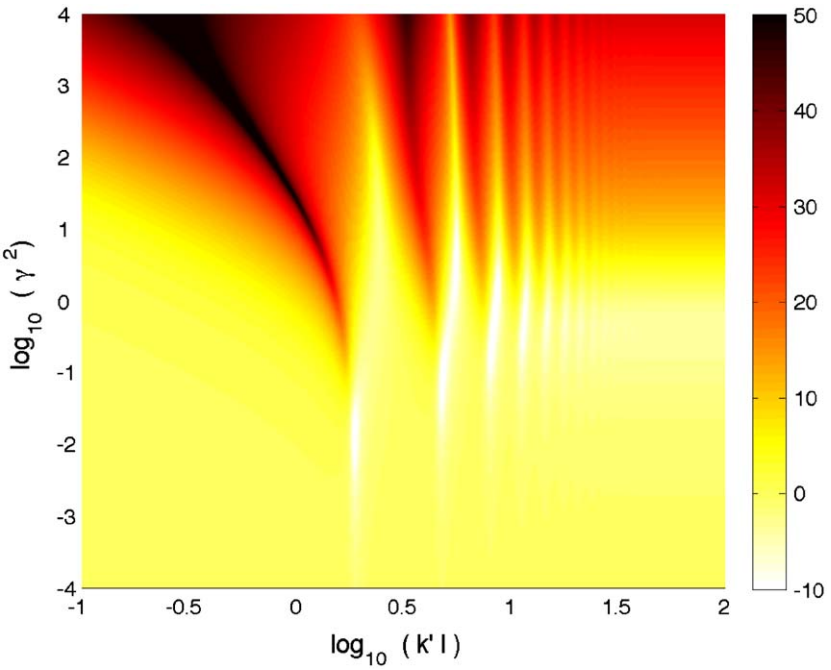

Fig. 11. The normalised active force in dB as a function of γ and kl, for $\beta^2 = 1$.

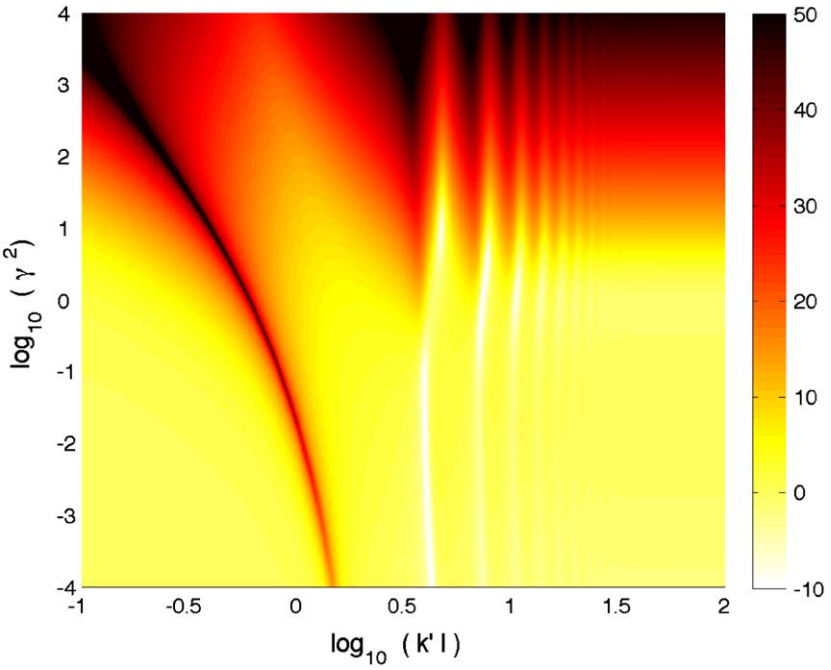

Fig. 12. The normalised active force in dB as a function of γ and kl, for $\beta^2 = 10$.

where $*$ denotes the complex conjugate. Through power conservation, the sum of the active power and the power dissipated in the resonant beam is equal to the incident wave power. Figs. 13–15 show the active power for the same parameter spaces as in previous figures. The left-hand figure shows the power level normalised by the power carried by an incident wave, and the right-hand figure shows the sign of the active power. A negative sign means that the active force absorbs and a positive sign means that the active force injects power. A low power level means that most of the incident power is dissipated passively in the resonant beam, and only a small part is absorbed by the active force.

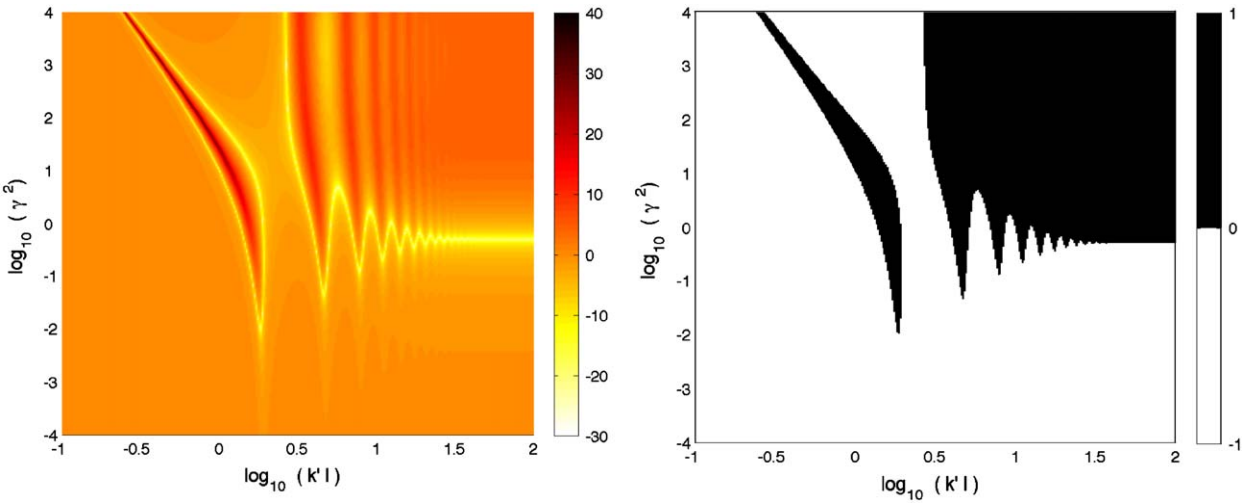

Fig. 13. The power absorbed or injected by the active force as a function of γ and kl for $\beta^2 = 0.1$. To the left: the power level normalised to the power carried by an incident wave; to the right: the sign of the power, -1 (white) means power is absorbed by the active force and $+1$ (black) means that power is injected.

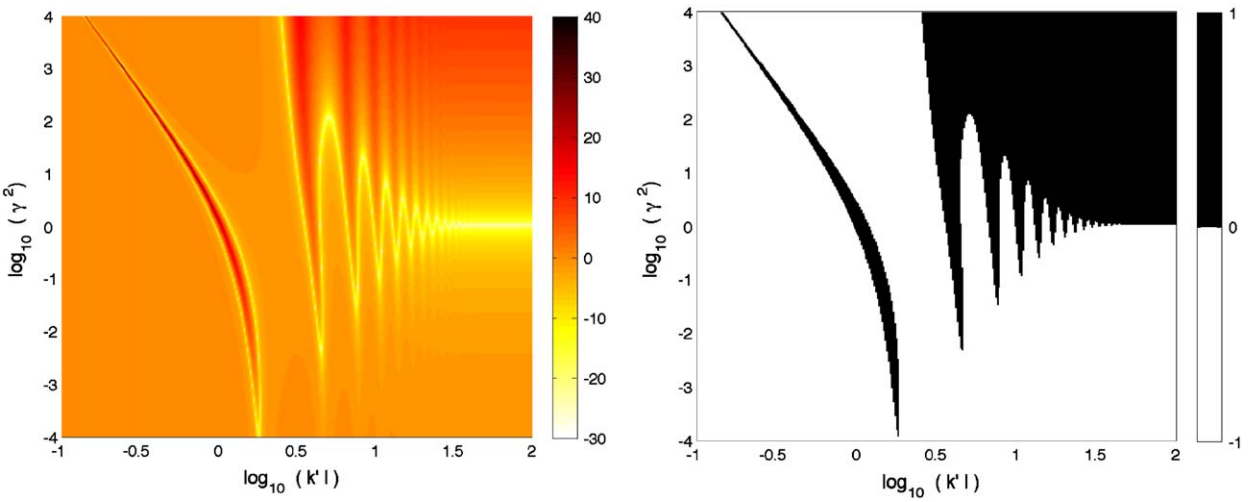

Fig. 14. The power absorbed or injected by the active force as a function of γ and kl for $\beta^2 = 1$. To the left: the power level normalised to the power carried by an incident wave; to the right: the sign of the power, -1 (white) means power is absorbed by the active force and $+1$ (black) means that power is injected.

Figs. 13–15 have large regions where the active force dissipates virtually all incident wave power, this corresponds to 0 dB and a negative sign. At some resonances, the active force does not absorb power but it injects power into the resonant beam (the black areas in the right-hand graphs in Figs. 13–15). Hence, the power injected by the active force in addition to the incident wave power is absorbed passively in the resonant beam. At corresponding resonances there is also a high control effort; see Figs. 10–12. The same phenomena were reported in [19]. For hybrid passive–active vibration control, the high control effort and power injection are not preferable. In the intersections between the regions in Figs. 13–15 where power is injected or absorbed, respectively, the active power changes sign and the power level reaches a minimum. Thus for these parameter values most of the incident wave power is dissipated in the resonant beam. These regions often correspond to regions in Figs. 10–12 with a low control effort. Regions with a low amount of actively absorbed power can be found in Figs. 13–15 also for low values of kl, for higher values of γ. Thus even in the case where the resonant beam is short in comparison to the wavelength, it offers high passive absorption in the presence of the active force. However, it may only be true for a narrow band of kl. Further, this may also require a high control effort which indicates that as a part of a hybrid passive–active vibration control system, a short and heavy resonant beam is not preferable.

It is possible to find combinations of β and γ which give the potential of a hybrid passive–active vibration control solution which may offer benefits compared to a purely passive or a purely active one. This implies a control effort that is

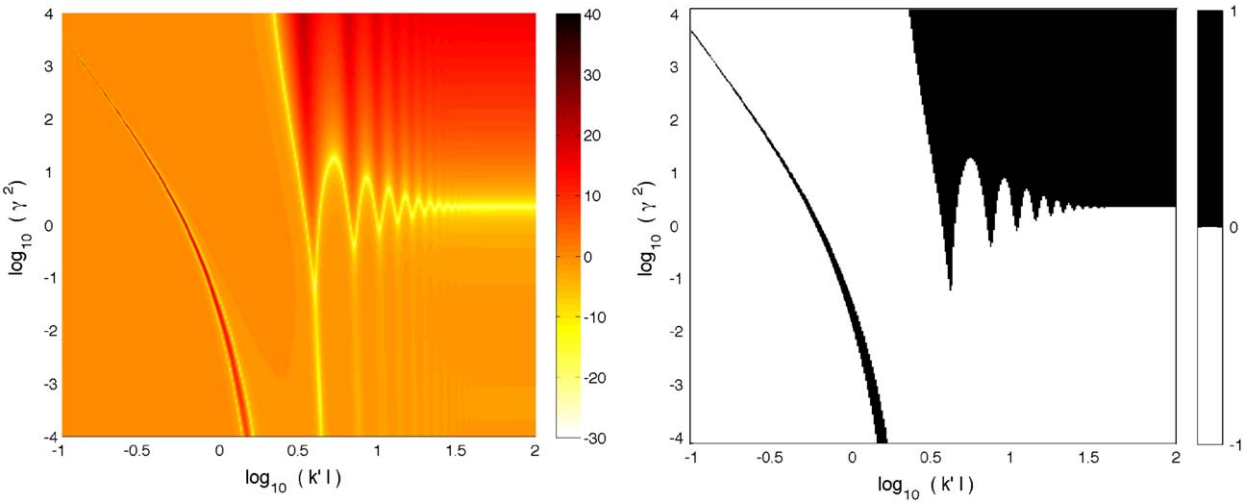

Fig. 15. The power absorbed or injected by the active force as a function of γ and kl for $\beta^2 = 10$. To the left: the power level normalised to the power carried by an incident wave; to the right: the sign of the power, -1 (white) means power is absorbed by the active force and $+1$ (black) means that power is injected.

lower than cancelling the reflection at a free end, and a passive power absorption which is substantially improved by the presence of the active force. One example is when $\beta^2 = 0.1$ and $\gamma^2 \approx 0.5$, i.e., the non-resonant beam has 10 times the stiffness and twice the mass of the resonant beam, and for high values of kl. In this case the passive junction absorbs about 70 percent of the incident wave power. When the active force acts on the system, the resonant beam (passive part of the hybrid system) absorbs virtually all the incident wave power (about 99 percent). Thus, the active force increases the efficiency of the passive damping but it does not absorb much power actively. In this case the control effort is about 60 percent of that absorbing all incident wave power actively at a free end. Thus, if the properties of the resonant beam are chosen appropriately, a hybrid passive–active vibration control configuration, such as the one presented, may offer an alternative to traditional passive solutions, purely active solutions or other hybrid solutions such as active constrained layers. However, it may only be advantageous for a limited frequency range (high values of kl).

4. Conclusions

This paper presents a theoretical study of the active control of flexural waves at a beam junction between a non-resonant and a resonant Euler–Bernoulli beam, where the resonant beam is considered to have structural damping while the non-resonant beam does not. First the reflection efficiency of the passive junction is studied for different properties of the resonant beam. The results confirm the expectation that high absorption of incident wave power (i.e. a low reflection efficiency) is achieved if the beams have similar stiffness and mass and if the resonant beam is long in comparison to the wavelength. However, high absorption could also be achieved in cases when the resonant beam is not very long compared to the wavelength, if the beams have a certain stiffness and mass ratio, and kl. In these cases, the resonant beam virtually works as a tuned vibration absorber. The results also show that when the beams have equal mass and stiffness there is an optimal choice of loss factor for each value of kl in order to minimise the reflection efficiency. It is not necessarily the highest loss factor that results in the highest absorption of incident wave power. A too high loss factor may increase the impedance mismatch at the junction.

An external force is introduced at the junction in order to make the junction non-reflective. The control effort and power injected or absorbed by the active force are studied for different properties of the resonant beam. The results show that for a certain ratio of bending stiffness and mass the presented hybrid passive–active solution may offer advantages, in term of efficiency and control effort, compared to purely passive or purely active solutions. However, this requires a quite specific design of the resonant beam. This might make such a hybrid configuration impractical for implementation. There is also a number of other issues that needs to be solved before considering an implementation. Issues such as stability of the control system, how the system matrices can be measured or estimated from measurements and in the latter case how such estimation errors might influence the control system.

Acknowledgement

This work has been funded by the Swedish research council, project: 621-2004-5185.

References

[1] D. Miller, A. von Flotow, A travelling wave approach to power flow in structural junctions, *Journal of Sound and Vibration* 128 (1989) 145–162.
[2] J. Moore, Vibration transmission through frame or beam junctions, *Journal of the Acoustical Society of America* 88 (1990) 2766–2776.
[3] L. Cremer, M. Heckl, *Körperschall*, Springer, Berlin, Heidelberg, 1967 (English edition: L. Cremer, M. Heckl, B.A.T. Peterson, Structure-borne sound, Springer, Berlin, Heidelberg, 2005).
[4] B.R. Mace, Wave reflection and transmission in beams, *Journal of Sound and Vibration* 97 (1984) 237–246.
[5] C. Mei, B.R. Mace, Wave reflection and transmission in Timoshenko beams and wave analysis of Timoshenko beam structures, *Transactions of the American Society of Mechanical Engineering* 127 (2005) 382–394.
[6] D. Miller, A. von Flotow, S. Hall, Active modification of wave reflection and transmission in flexible structures, *Proceedings of the 1987 American Control Conference*, 1987.
[7] D. Miller, S. Hall, A. von Flotow, Optimalcontrol of power flow at structural junctions, *Journal of Sound and Vibration* 140 (1990) 475–497.
[8] D. Miller, *Modelling and Active Modification of Wave Scattering in Structural Networks*, Ph.D. Thesis, Massachussets Institute of Technology, 1988.
[9] J. Scheuren, Non-reflecting termination for bending waves in beams by active means, *Proceedings of Inter-Noise in Avignon*, 1988.
[10] J. Scheuren, Activeattenuation of bending waves in beams, *Proceedings of the Spring Conference of the Institute of Acoustics in Southampton*, 1990.
[11] A. von Flotow, B. Schäfer, Wave-absorbing controllers for a flexible beam, *Journal of Guidance* 9 (1986) 673–680.
[12] D. Guicking, J. Melcher, R. Wimmel, Active impedance control in mechanical structures, *Acustica* 69 (1989) 39–52.
[13] R. Gonzalez, F.O. Bustamente, Active control of the reflection of waves in beams, *Proceedings of SPIE—The International Society for Optical Engineering*, 2001, pp. 587–596.
[14] M.J. Brennan, S.J. Elliot, R.J. Pinnington, Strategies for the active control of flexural vibration on a beam, *Journal of Sound and Vibration* 186 (1995) 657–688.
[15] B.R. Mace, Active control of flexural vibrations, *Journal of Sound and Vibration* 114 (1987) 253–270.
[16] R.J. McKinnel, Active vibration isolation by cancelling bending waves, *Proceeding of the Royal Society of London* 421 (1989) 357–393.
[17] C.R. Halkyard, B.R. Mace, Adaptive active control of flexural waves in a beam in the presence of near-fields, *Journal of Sound and Vibration* 285 (2005) 149–171.
[18] J.L. Svensson, P.B.U. Andersson, J. Scheuren, W. Kropp, Active scattering control of flexural waves at beam junctions—the influence of beam properties on power flow and control effort, *Journal of Sound and Vibration* 313 (2008) 418–432.
[19] J.L. Svensson, P.B.U. Andersson, J. Scheuren, W. Kropp, Feedforward control of bending waves in frequency domain at structural junctions using an impedance formulation, *Journal of Sound and Vibration* 323 (2009) 555–573.
[20] S. Beyene, R.A. Burdisso, A new hybrid passive/active noise absorption system, *Journal of the Acoustical Society of America* 101 (1997) 1512–1515.
[21] M. Furstoss, D. Thenail, M.A. Galland, Surface impedance control for sound absorption: direct and hybrid passive/active strategies, *Journal of Sound and Vibration* 203 (1997) 219–236.
[22] J. Smith, B. Johnson, R. Burdisso, A broadband passive–active sound absorption system, *Journal of the Acoustical Society of America* 106 (1999) 2646–2652.
[23] J. Yuan, Causal impedance matching for broadband hybrid noise absorption, *Journal of the Acoustical Society of America* 113 (2003) 3226–3232.
[24] A. Baz, Active constrained layer damping, *Damping'93 conference*, Vol. 3, San Francisco, CA, 1993, IBB 1–23.
[25] A. Baz, J.J. Ro, The concept and performance of active constrained layer damping treatments, *Sound and Vibration* 2193 (1994) 98–114.
[26] W.H. Liao, K.W. Wang, Characteristics of enhanced active constrained layer damping treatments with edge elements, Part 1: finite element model development and validation, *Journal of Vibration and Acoustics* 120 (1998) 886–893.
[27] W.H. Liao, K.W. Wang, Characteristics of enhanced active constrained layer damping treatments with edge elements, Part 2: system analysis, *Journal of Vibration and Acoustics* 120 (1998) 894–900.
[28] Y. Liu, K.W. Wang, Damping optimization by integrating enhanced active constrained layer and active–passive hybrid constrained layer treatments, *Journal of Sound and Vibration* 255 (2002) 763–775.
[29] H. Illare, W. Kropp, Quantification of damping mechanisms of active constrained layer treatments, *Journal of Sound and Vibration* 1–2 (2005) 189–217.
[30] M.J. Lam, D.J. Inman, W.R. Saunders, Vibration control through passive constrained layer damping and active control, *Journal of Intelligent Material Systems and Structures* 8 (1997) 663–677.
[31] H. Illare, *A Study of Active–Passive Damping Treatments*, Ph.D. Thesis, Chalmers University of Technology, 2004.
[32] X. Pan, C.H. Hansen, Effect of end conditions on the active control of beam vibration, *Journal of Sound and Vibration* 168 (1993) 429–448.
[33] J.L. Svensson, An impedance approach to passive-active vibration control, Technical Report, Division of Applied Acoustics, Chalmers University of Technology, 2008.
[34] C.H. Hansen, S.D. Snyder, *Active Control of Noise and Vibration*, E and FN Spon, 1997.
[35] H.M. El-Khatib, B.R. Mace, M.J. Brennan, Suppression of bending waves in a beam using a tuned vibration absorber, *Journal of Sound and Vibration* 288 (2005) 1157–1175.
[36] S.J. Elliot, L. Billet, Adaptive control of flexural waves propagating in a beam, *Journal of Sound and Vibration* 162 (1993) 295–310.
[37] M.J. Brennan, J. Garcia-Bonito, S.J. Elliot, A. David, R.J. Pinnington, Experimental investigation of different actuator technologies for active vibration control, *Smart Materials and Structures* 8 (1999) 145–153.